Magnetic phase diagram of the quantum spin chain compound $SrCo_2V_2O_8$

A single-crystal neutron diffraction study

Shen, L.; Zaharko, O.; Birk, Jonas Okkels; Jellyman, E.; He, Z.; Blackburn, E.

Published in:
New Journal of Physics

DOI:
10.1088/1367-2630/ab2b7a

2019

New Journal of Physics
The open access journal at the forefront of physics

Deutsche Physikalische Gesellschaft DPG IOP Institute of Physics

PAPER • OPEN ACCESS

Magnetic phase diagram of the quantum spin chain compound $SrCo_2V_2O_8$: a single-crystal neutron diffraction study

To cite this article: L Shen *et al* 2019 *New J. Phys.* **21** 073014

New Journal of Physics
The open access journal at the forefront of physics

Deutsche Physikalische Gesellschaft DPG
IOP Institute of Physics

Published in partnership with: Deutsche Physikalische Gesellschaft and the Institute of Physics

OPEN ACCESS

RECEIVED
20 February 2019

REVISED
27 May 2019

ACCEPTED FOR PUBLICATION
20 June 2019

PUBLISHED
3 July 2019

PAPER

Magnetic phase diagram of the quantum spin chain compound $SrCo_2V_2O_8$: a single-crystal neutron diffraction study

L Shen[1,2,3,4], **O Zaharko**[5], **J O Birk**[5], **E Jellyman**[1], **Z He**[6] **and E Blackburn**[1,2]

[1] School of Physics and Astronomy, University of Birmingham, Birmingham B15 2TT, United Kingdom
[2] Division of Synchrotron Radiation Research, Lund University, SE-22100, Lund, Sweden
[3] Stanford Institute for Materials and Energy Science, Stanford University and SLAC National Accelerator Laboratory, Menlo Park, CA 94025, United States of America
[4] Linac Coherent Light Source, SLAC National Accelerator Laboratory, 2575 Sand Hill Road, Menlo Park, CA 94025, United States of America
[5] Laboratory for Neutron Scattering and Imaging, Paul Scherrer Institut, CH-5232 Villigen PSI, Switzerland
[6] State Key Laboratory of Structural Chemistry, Fujian Institute of Research on the Structure of Matter, Chinese Academy of Sciences, Fuzhou, Fujian 350002, People's Republic of China

E-mail: lingjia.shen@sljus.lu.se

Keywords: low dimensional quantum magnetism, magnetic-field-induced phase transitions, quantum criticality

Abstract

We explore magnetic order in the quantum spin chain compound $SrCo_2V_2O_8$ up to 14.9 T and down to 50 mK, using single-crystal neutron diffraction. Upon cooling in zero-field, commensurate antiferromagnetic (C-AFM) order with modulation vector $\boldsymbol{k}_C = (0, 0, 1)$ develops below $T_N \simeq 5.0$ K. Applying an external magnetic field ($H \| c$ axis) destabilizes this C-AFM order, leading to an order-disorder transition between T_N and ~1.5 K. Below 1.5 K, a commensurate to incommensurate (IC-AFM) transition occurs at 3.9 T, above which the magnetic reflections can be indexed by $\boldsymbol{k}_{IC} = (0, 0, 1 \pm \delta l)$. The incommensurability δl scales monotonically with H until the IC-AFM order disappears around 7.0 T. Magnetic reflections modulated by $\boldsymbol{k}_C$ emerge again at higher fields. While the characters of the C-AFM, IC-AFM and the emergent AFM order in $SrCo_2V_2O_8$ appear to fit the descriptions of the Néel, longitudinal spin density wave and transverse AFM order observed in the related compound $BaCo_2V_2O_8$, our results also reveal several unique signatures that are not present in the latter, highlighting the inadequacy of mean-field theory in addressing the complex magnetic order in systems of this class.

1. Introduction

Magnetic field is a very important parameter when tuning the physical properties in quasi one-dimensional (1D) spin-1/2 magnets. The magnetic excitation spectrum of a single quantum chain is a continuum composed of pairs of spinons, each with $S = 1/2$, that can propagate like domain walls [1]. In quasi 1D magnets where there are non-zero interactions between the chains, the spinons become confined by an attractive potential [2]. Concomitantly, the continuum spectrum is replaced by a series of discrete spinon bound states. It has been found that the spinon confinement can be significantly tuned by applying a magnetic field [3–7].

Furthermore, exotic magnetic long-range order (LRO) may appear in a magnetic field. For example, in weakly coupled spin chains or ladders with a singlet-dimer ground state ($S = 0$), applying a magnetic field splits the associated triplet excitation ($S = 0, \pm 1$); a singlet-dimer to LRO transition occurs at the closure of the energy gap corresponding to the lowest triplet branch ($S = 1$). This transition, also known as magnon Bose–Einstein condensation (BEC), has been intensively studied in the last two decades [8–10].

Recently, the weakly coupled quantum spin chain compound $SrCo_2V_2O_8$ has raised much attention due to the exotic magnetism that it hosts, including the magnetic-field-induced order-disorder transition [11], spinon confinement [5, 12] and Bethe strings [7]. This compound crystallizes in a body-centred tetragonal lattice (space group $I4_1cd$), in which 4-fold screw chains of CoO_6-octahedra run along the crystallographic c-axis [13, 14]. These chains are well separated in the ab plane, greatly reducing the strength of the interactions between the

chains. The Co^{2+} ion ($3d^7$) has an effective spin of 1/2 because of the octahedral distortion and spin–orbit coupling [15, 16]. The intrachain spin interactions in $SrCo_2V_2O_8$ can be described by an *XXZ* model written as

$$\mathcal{H}_{XXZ} = J\sum_i \{S_i^z S_{i+1}^z + \epsilon (S_i^x S_{i+1}^x + S_i^y S_{i+1}^y)\} - g_z \mu_B \sum_i S_i^z H, \quad (1)$$

where $J > 0$ is the nearest-neighbour (NN) antiferromagnetic (AFM) exchange constant, ϵ is the anisotropy parameter, and g_z is the component of the Landé *g*-tensor along the chain direction [5, 7, 12]. This Hamiltonian can be exactly solved by the Bethe ansatz [17]. The anisotropy in $SrCo_2V_2O_8$ is Ising-like ($\epsilon < 1$) [5, 7, 12–14], for which the *XXZ* model predicts a Néel type AFM ground state. A spin disordered state, described as a Tomonaga–Luttinger liquid (TLL), can be induced above a critical magnetic field. The spinon spectrum in the TLL state of an Ising-like *XXZ* spin chain is dominated by a longitudinal (transverse) mode in the intermediate (high) magnetic field region [18, 19]. In a quasi 1D system, the interchain exchange interactions come into play at low temperatures. Consequently, the longitudinal (transverse) mode is expected to condense, giving rise to a longitudinal spin density wave (LSDW) (transverse AFM) state. In $MCo_2V_2O_8$ (M = Sr, Ba), this spin density wave should be characterized by an incommensurate modulation vector (δl),

$$|\delta l| = 4 \times \langle S_z \rangle = 4 \times M_z / g_z \mu_B, \quad (2)$$

where M_z is the uniform magnetization along the chain direction [20, 21].

In $SrCo_2V_2O_8$, the interchain exchange interactions are nonnegligible, leading to the occurrence of Néel order at a finite temperature $T_N = 5.0$ K [13, 14]. Theoretically, Okunishi and Suzuki have used bosonization combined with a mean-field treatment of the interchain interactions to study the magnetic phase diagram in $MCo_2V_2O_8$ (M = Sr, Ba) [22]. At very low temperatures, they obtained a LSDW phase that replaces the Néel order above an intermediate critical field, and another LSDW to transverse AFM phase transition in the high field region. So far, the exotic magnetic-field-induced phases have only been confirmed in the Ba-compound by single-crystal neutron diffraction [20, 21, 23, 24]. These studies have revealed that the critical field for the Néel to LSDW transition (~3.9 T) agrees well with the mean-field prediction, while the one for the LSDW to transverse AFM transition (~9.0 T) appears to be much lower than the predicted value (~15.1 T). The discrepancy might indicate that the inter- and intra-chain exchange parameters used in [22] are not correct [24] or that the mean-field theory is inadequate. As pointed out by a recent nuclear magnetic resonance (NMR) study, the intra- and inter-couplings in $BaCo_2V_2O_8$ are rather complicated and could be strongly field-dependent [25].

The static magnetic order in $SrCo_2V_2O_8$ has only been investigated in zero-field by neutron powder diffraction [14], while its evolution in a longitudinal magnetic field, especially in the low temperature region where the LSDW and transverse AFM are predicted to develop [22], is not known. To further check the mean-field theory, and more importantly, obtain more insights into the magnetic properties in materials of this class, we report the magnetic phase diagram of $SrCo_2V_2O_8$ up to 14.9 T ($H \| c$ axis) and down to 50 mK, using single-crystal neutron diffraction. Our experimental results are organized into two sections. The first focuses on the commensurate (C) AFM order and magnetic-field-induced order-disorder transition above 2.0 K (section 3). The second looks at the phase diagram below 2.0 K for fields up to 14.9 T, covering a magnetic-field-induced incommensurate (IC) AFM order (3.9 T $< \mu_0 H <$ 7.0 T) and emergent commensurate antiferromagnetic (C-AFM) order ($\mu_0 H >$ 7.0 T) (section 4). Finally, in section 5, we will discuss several unique signatures of the spin states in $SrCo_2V_2O_8$ that are not present in $BaCo_2V_2O_8$.

2. Experimental methods

Two high quality $SrCo_2V_2O_8$ single crystals (~3 × 3 × 6 mm^3) were measured in this investigation. They were grown by the spontaneous nucleation method described in [13]. All single-crystal neutron diffraction measurements were carried out at the Swiss Spallation Neutron Source (SINQ) at the Paul Scherrer Institute. Both single crystals were aligned using the two-axis neutron diffractometer ORION. The first single-crystal was mounted into a dilution refrigerator and then into a 6 T vertical cryomagnet, with the magnetic field applied along the *c*-axis. This was installed on the thermal neutron diffractometer TriCS and measured with a lifted detector (normal beam geometry). For the magnetic structure determination, a set of magnetic and nuclear reflections were collected at neutron wavelength $\lambda = 1.178$ Å using a Ge(311) monochromator. All the other measurements were performed at $\lambda = 2.317$ Å using a PG(002) monochromator with a vertical 80′ collimator installed to improve the resolution along the $\mathbf{c}^*$ direction in the reciprocal space.

The second crystal was mounted in a 15 T vertical cryomagnet equipped with a dilution refrigerator insert and then measured on the cold triple-axis spectrometer RITA-II. The *c*-axis was aligned along the magnetic field. The incident neutron energy was fixed at 5 meV using a vertically focusing PG(002) monochromator. The energy of the scattered neutrons was analysed using a multi-blade PG(002) crystal analyser, which was operated in a monochromatic imaging mode [26]. A cooled beryllium filter was placed between the sample and analysers

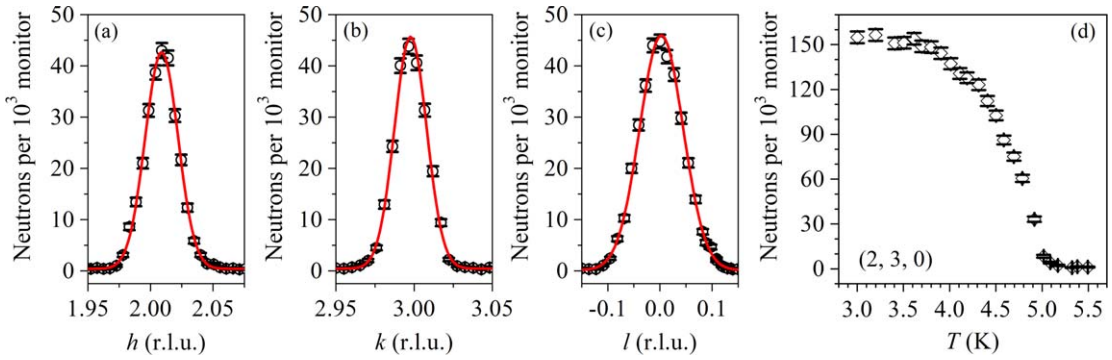

Figure 1. (a)–(c) Open symbols: *hkl*-scans performed at $T = 50$ mK and $\mu_0 H = 0$ T. The red lines are numerical fits using a Gaussian function. (d) Temperature dependence of the peak intensity of the (2, 3, 0) reflection at $\mu_0 H = 0$ T.

Table 1. Basis functions Ψ_n ($n = 1, ..., 12$) of Co for the irreducible representation Γ_5. The basis functions contributing to a finite moment in the *ab* plane are highlighted in grey. The atomic sites are labelled as Co_1: (x, y, z), Co_2: $(-x + 1, -y + 1, z)$, Co_3: $(-y + 1, x + 1/2, z + 1/4)$, Co_4: $(y, -x + 1/2, z + 1/4)$, Co_5: $(-x + 1, y, z + 1/2)$, Co_6: $(x, -y + 1, z + 1/2)$, Co_7: $(y + 1/2, x, z + 1/4)$, and Co_8: $(-y + 1/2, -x + 1, z + 1/4)$.

Site label	Ψ_1	Ψ_2	Ψ_3	Ψ_4	Ψ_5	Ψ_6	Ψ_7	Ψ_8	Ψ_9	Ψ_{10}	Ψ_{11}	Ψ_{12}
Co_1	100	010	001	000	000	000	000	000	000	100	010	001
Co_2	100	010	00−1	000	000	000	000	000	000	100	010	00−1
Co_3	010	−100	001	000	000	000	000	000	000	0−10	100	00−1
Co_4	010	−100	00−1	000	000	000	000	000	000	0−10	100	001
Co_5	000	000	000	−100	010	001	−100	010	001	000	000	000
Co_6	000	000	000	−100	010	00−1	−100	010	00−1	000	000	000
Co_7	000	000	000	010	100	001	0−10	−100	00−1	000	000	000
Co_8	000	000	000	010	100	00−1	0−10	−100	001	000	000	000

to suppress the $\lambda/2$ contamination. The neutrons were detected using a position-sensitive detector (PSD) consisting of 128 × 128 pixels. In all measurements, only the elastic scattering signal was recorded.

3. Néel order and magnetic-field-induced order-disorder transition above 2.0 K

Several crystallographically forbidden reflections are observed at $T = 50$ mK and $\mu_0 H = 0$ T. They can be indexed by the commensurate modulation vector $k_C = (0, 0, 1)$, which is consistent with the Néel order reported in the previous neutron powder diffraction study [14]. Figures 1(a)–(c) shows cuts through the (2, 3, 0) reflection, measured on TriCS. Each peak was fitted using a Gaussian function, giving full width at half maximum (FWHM) values of 0.0310(5), 0.0242(4), and 0.098(1) r.l.u. for the *h*-, *k*-, and *l*-scans, respectively. These values serve as the TriCS instrumental resolution parameters around this particular momentum transfer referred to below. The temperature dependence measurements reveal that this reflection disappears around 5.0 K (figure 1(d)), which agrees with the T_N extracted from a previous heat capacity investigation on the same crystal [13].

To study the magnetic structure in the Néel phase, we carried out a representational analysis using the SARAh Representational Analysis software [27]. Five irreducible representations (Γ_n, $n = 1, 2, 3, 4, 5$) could be obtained [14]. Γ_1, Γ_2, Γ_3, and Γ_4 did not yield satisfactory agreements to our data. This leaves Γ_5 (table 1) for our refinement, which is consistent with the conclusion in a neutron powder diffraction study [14]. For the nuclear structure, we have collected 17 reflections to refine the scale factor, while the atomic positions and isotropic atomic displacement parameters were fixed to the values reported in [14].

We have collected 46 magnetic reflections for the magnetic structure determination at 50 mK and 0 T. We first discuss the two-domain solution proposed in [21]; the corresponding magnetic structures are illustrated in figures 2(a) and (b). This scenario is allowed because the basis functions of Co_n ($n = 1$–4) are independent of those of Co_n ($n = 5$–8) (table 1). Following this approach, we constrain all the Co sites to have an identical amplitude of magnetic moment, while their orientations are decided by symmetry [21]. Initially, we included all the basis functions of Γ_5 in the refinement. The coefficients for the ones contributing to a finite moment in the *ab* plane (highlighted in grey in table 1) were found to be too weak to be resolved from our data, but we cannot exclude their existence. This agrees well with the Ising-like anisotropy revealed in the magnetization and

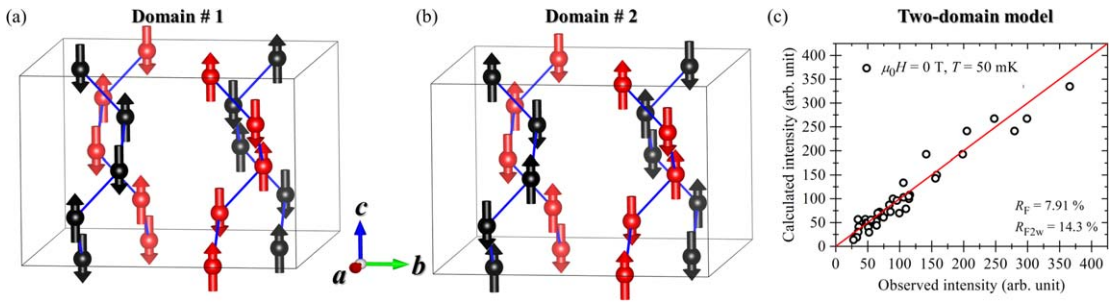

Figure 2. (a)–(b) Magnetic structure of $SrCo_2V_2O_8$ in the two magnetic domains of the Néel phase. The screw chains formed by Co_n (n = 1–4) and Co_n (n = 5–8) sites are marked in red and black, respectively. (c) Magnetic structure refinement in the Néel phase at T = 50 mK and μ_0H = 0 T. The R-factors (R_F, R_{F2w}) which characterise the quality of our refinement are also listed.

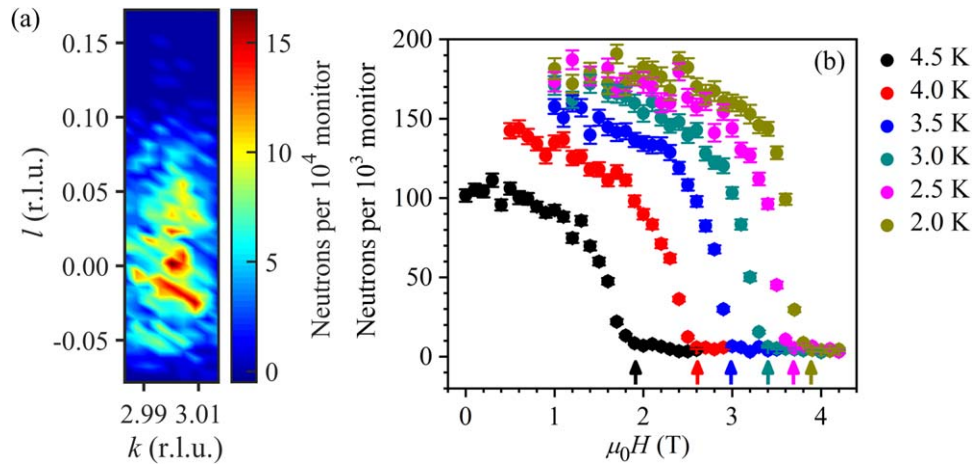

Figure 3. (a) The diffraction pattern of the (2, 3, 0) reflection recorded using a PSD [26] at 4.0 K and 0.5 T. The streak-like nature is an artifact of the vertically focusing monochromator. (b) The summed intensity of (2, 3, 0) between 2.0 and 4.5 K as a function of magnetic field.

neutron powder diffraction studies [11, 14]. Moreover, we could not detect any contribution from Ψ_6 and Ψ_{12} within the resolution. As a result, only Ψ_3 and Ψ_9 were adopted in our final refinement; this fits the description of the Néel order predicted by equation (1), wherein the spins are antiferromagnetically coupled along the chain (figures 2(a) and (b)). As shown in figure 2(c), the two-domain solution reproduces the experimental observations well. The domain populations in our sample are 42(3)% and 58(3)% for Domain #1 and Domain #2 (figures 2(a) and (b)), respectively. The refined moment along the c axis is 1.81(4) μ_B per Co. We note that this value is lower than the 2.1–2.3 μ_B per Co at 1.5 K reported in the powder study [14], which may be due to variation in the sample quality.

Our single crystal data allows us to test a single-domain solution in which the aforementioned moment constraint for the Co sites is released [21]. We obtained 2.6(1) and −0.20(9) μ_B for the Co_n (n = 1–4) and Co_n (n = 5–8) sites (table 1), respectively. Since the single-domain refinement also reproduces the experimental observations well (R_F = 7.85%, R_{F2w} = 14.6%), we cannot rule out this possibility. Local probes, such as NMR [28], are needed to further clarify the magnetic structure in this compound in the future.

While applying a magnetic field ($H \| c$ axis), magnetization and heat capacity measurements suggest that $SrCo_2V_2O_8$ undergoes a field-induced order-disorder transition between T_N and 2.0 K [11]. We studied the magnetic field dependence of the (2, 3, 0) reflection using the PSD on RITA-II. A typical diffraction pattern measured at 4.0 K and 0.5 T is shown in figure 3(a). We then studied the magnetic field dependence of this reflection at several temperatures between 2.0 and 4.5 K. These observations are summarized in figure 3(b). A field-induced order-disorder transition, which has been observed in the sister compound $BaCo_2V_2O_8$ [21, 29, 30], is also clearly present in $SrCo_2V_2O_8$. We note that we could not detect any field-induced change in the magnetic modulation vector at all temperatures and fields discussed in this section.

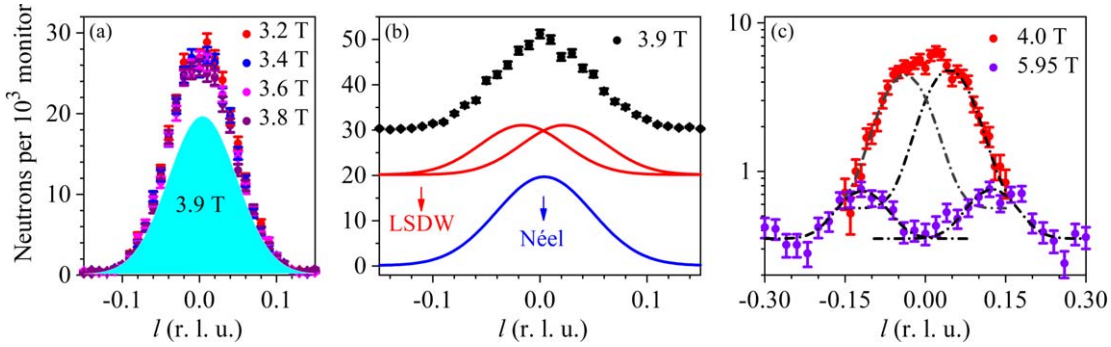

Figure 4. Magnetic field dependence of the (2, 3, l) reflection (l-scan) at 75 mK and (a) 3.2 T $\leqslant \mu_0 H \leqslant$ 3.8 T, (b) $\mu_0 H = 3.9$ T, and (c) $\mu_0 H = 4.0$ and 5.95 T. The shaded area in (a) denotes the fit to the data at 3.9 T for comparison. The curves displayed in (b) have been shifted vertically. The solid lines in (b) and (c) are numerical fits (see the main text). The counting time for each 10^3 neutron monitor is about 0.34 s.

4. Magnetic-field-induced phase transitions below 2.0 K

We now study the magnetic field response of the C-AFM order at temperatures down to 50 mK. Figure 4 shows the (2, 3, l) reflection at 75 mK measured between 3.2 and 5.95 T on TriCS. Below 3.9 T, this reflection hardly changes and is centred at $l = 0$ (figure 4(a)). The average FWHM of the peaks in this region is 0.098 r.l.u.; it is equal to the instrumental resolution within the errors (see section 3). At 3.9 T, the intensity weakens (figure 4(a)). At higher fields, we clearly see two peaks modulated by $\boldsymbol{k}_{\rm IC} = (0, 0, 1 \pm \delta l)$, featuring an IC-AFM phase (figure 4(c)). While magnetic refinement is needed to properly determine the nature of this IC-AFM order, one plausible scenario, based on the splitting of the magnetic reflection along $\mathbf{c}^\star$, is LSDW order, as demonstrated in the related compound $BaCo_2V_2O_8$ [20, 21].

We have fitted the magnetic reflection at 3.9 T using three models (figure 4(b)). In the first model, we apply a single Gaussian function centred at $l = 0$ to this profile, meaning that the system is still in the C-AFM state. We obtain a broadened reflection with FWHM $= 0.105(2)$r.l.u. (figure 4(b)). In the second model, we apply two Gaussian functions centred at $l = \pm\delta l$. This model, which produces a FWHM of 0.09(1) r.l.u., corresponds to a single IC-AFM phase (figure 4(b)). The third model, in which we assume the coexistence of the C-AFM and IC-AFM reflections, gives a FWHM of 0.07(1)r.l.u. This value is much smaller than the instrumental resolution 0.098(1)r.l.u. (section 3); we therefore rule out the third model. While the second model fits the observations in $BaCo_2V_2O_8$ [20, 23], we cannot rule out the presence of a short-range ordered C-AFM phase at 3.9 T within the experimental resolution.

We could only resolve the two IC reflections when $\mu_0 H \geqslant 4.0$ T, based on which we conclude that the IC-AFM state sets in around 3.9 T in $SrCo_2V_2O_8$. The IC peak is resolution limited in an l-scan at all magnetic fields measured, indicating long-range spin correlation along the c-axis. This is consistent with the observations of the LSDW order in $BaCo_2V_2O_8$ [20, 21]. The IC reflection could be detected up to the highest field measured on TriCS (5.95 T). We also tracked the temperature dependence of this phase. These results are summarized in the magnetic field versus temperature phase diagram displayed in figure 8 later in the paper.

To explore the evolution of the IC-AFM order above 5.95 T in $SrCo_2V_2O_8$, we performed further measurements on RITA-II using a 15 T vertical cryomagnet. Neither the cryomagnet nor detector could be tilted, meaning that the neutron scattering intensity from the IC-AFM structure will be weakened by the Lorentz factor. However, by taking advantage of the PSD, we were still able to resolve a partial IC diffraction spot, and thus track its evolution.

Based on the data from TriCS, the diffraction spot of the (2, 3, 0) reflection in the PSD is expected to split vertically, i.e. along $\mathbf{c}^\star$, as the magnetic field is driven across the C-AFM to IC-AFM phase boundary. At 6.0 T, while the $-\delta l$ satellite peak goes out of the detection range of the PSD, the $+\delta l$ satellite peak can be clearly observed (figure 5(a)). The split can be resolved up to 6.5 T. Interestingly, the (2, 3, 0) reflection is recovered above 7.0 T (figure 5(a)). Due to the geometry limitation of the 15 T cryomagnet, we could not check the scattering signal in an extensive reciprocal space region. As a result, a multi-k modulation cannot be ruled out for the high field emergent phase. However, similar reentrant behaviour has been observed in $BaCo_2V_2O_8$ and was interpreted as a sign of the LSDW to transverse AFM order crossover [24]. We plot the summed intensity versus magnetic field curve in figure 5(b), in which the drastic drop above 4.0T fits the C-AFM to IC-AFM order transition illustrated in figure 4. We note that the rate of this drop is overestimated due to the fact that only the partial double peak profiles could be resolved above 5.0 T (figure 5(a)). The intensity reaches its minimum at 7.0 T, after which it increases monotonously with the magnetic field until 12.5 T. The reemergence of the

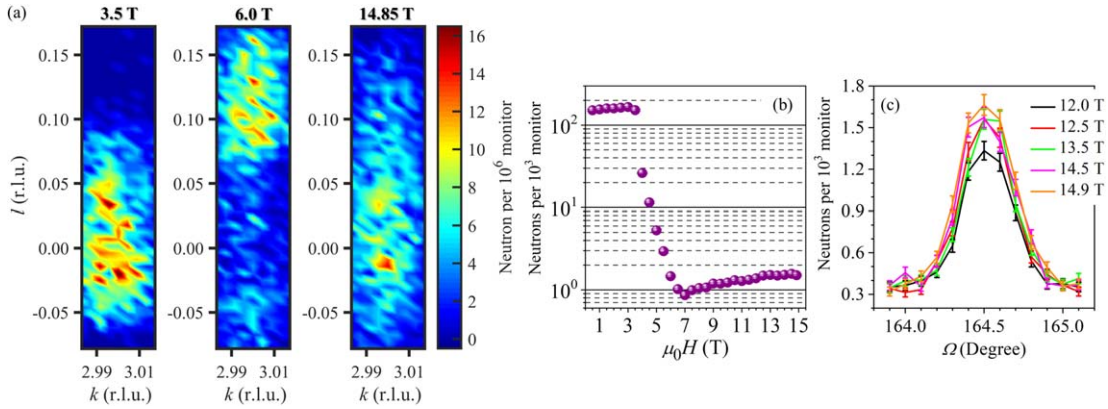

Figure 5. (a) The (2, 3, 0) reflection at selective magnetic fields. A scale factor of 1/100 has been applied to the data at 3.5 T. (b) Magnetic field dependence of the summed intensity. (b) Rocking curves of the (2, 3, 0) reflection for $\mu_0 H \geqslant 12.0$ T. All the data were collected at 120 mK.

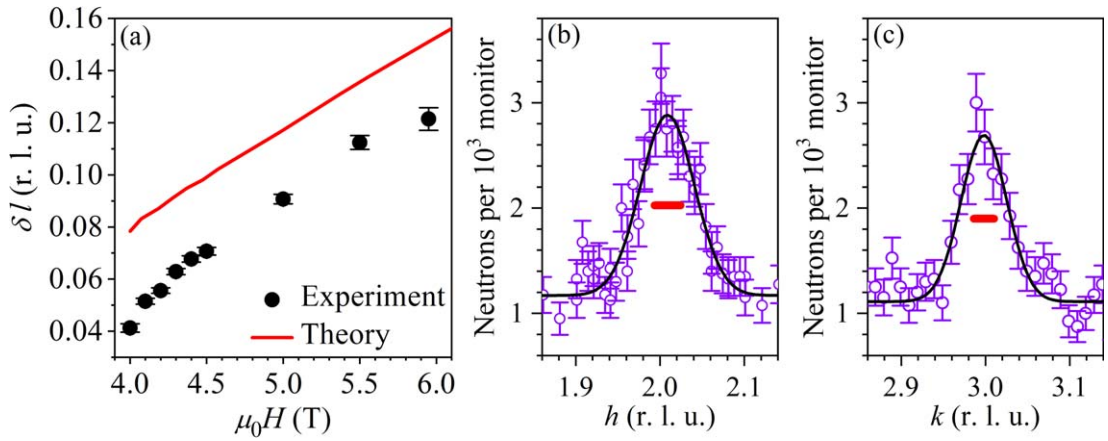

Figure 6. (a) Magnetic field dependence of the incommensurate propagation vector δl at 75 mK. The filled circles are the experimental observations, and the red line is the theoretical values deduced from equation (2) and [31]. (b) h- and (c) k-scans of the (2, 3, δl) reflection at $\mu_0 H = 5.0$ T and $T = 150$ mK. The black lines are Gaussian fits. The red bars are the instrumental resolution determined at zero field (see section 3).

scattering intensity above 7.0 T (figure 5(b)) is also consistent with the transverse AFM order observed in $BaCo_2V_2O_8$ [24]. At 7.0 T, we performed two additional measurements with a much longer counting time. We could resolve a signal at 100 mK, which fades away at 750 mK. However, this signal is too weak to check the coexistence of the IC-AFM and emergent AFM order reported in $BaCo_2V_2O_8$ [24]. The emergent AFM order in $SrCo_2V_2O_8$ is fully stabilized at 12.5T and above; the intensity remains unchanged up to the highest field probed (14.9 T, see figure 5(c)).

5. Discussion

In the IC-AFM state, increasing the magnetic field pulls the two IC peaks further apart (figure 4(c)). It has been proposed that the IC-AFM order results from the condensation of the longitudinal spin fluctuation of a TLL, meaning that its incommensurability δl should exactly follow equation (2) [20–23]; this has been verified in $BaCo_2V_2O_8$ [20, 21]. To check this scenario in $SrCo_2V_2O_8$, we compare our fitted δl at 75 mK with the values predicted by equation (2) (figure 6(a)). In this plot, the Landé g-tensor along the c axis ($g_c = 6.1$), Van Vleck paramagnetism correction factor (0.014 μ_B/T) and longitudinal uniform magnetization M_z measured between 1.3 and 1.9 K were used to produce the theoretical δl; these values have been reported in [31]. In sharp contrast to the good match between the experiment and theory in $BaCo_2V_2O_8$ [20, 21], all the observed δl in $SrCo_2V_2O_8$ are much lower than the predicted values (figure 6(a)). This discrepancy casts some doubt on the applicability of the TLL theory in interpreting the IC-AFM order in this case. However, the low-energy fractional magnetic excitations in this compound, e.g. spinons, (anti)psinons and Bethe strings, have been proven to be well

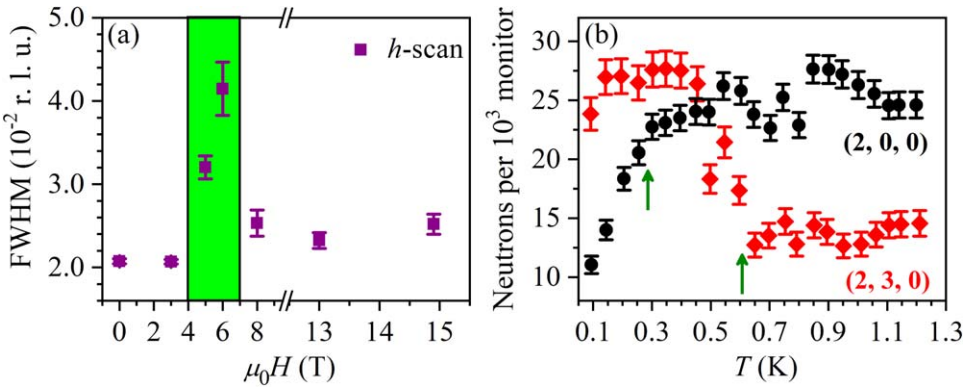

Figure 7. (a) Magnetic field dependence of the FWHM of the (2, 3, 0) reflection at 120 mK measured in a *h*-scan on RITA-II. The green shaded area marks the LSDW region. (b) Temperature dependence of the (2, 0, 0) and (2, 3, 0) reflections at 7.5 T. A scale factor of 40 has been applied to the (2, 3, 0) reflection. The green arrows mark the transition temperatures described in the main text.

described by equation (1) [5, 7, 12]. Moreover, the Néel ordering temperature of $SrCo_2V_2O_8$ ($T_N = 5.0$ K) is lower than that of $BaCo_2V_2O_8$ ($T_N = 5.5$ K) [21], supporting the stronger 1D character in the former. Based on these facts, it is less likely that the TLL theory fails in $SrCo_2V_2O_8$. We therefore propose another possible explanation here. The magnetization measurements for obtaining g_c and M_z were performed between 1.3 and 1.9 K [31]. To study M_z at lower temperatures, we measured the nuclear reflections (2, 0, 0) and (4, 0, 0). At high fields, additional neutron counts can be resolved on top of (2, 0, 0), while (4, 0, 0) is not affected up to 14.9 T (not shown here). This indicates the ferromagnetic origin of the weak field-induced intensity at (2, 0, 0) [21, 24]; the non-resolvable change at (4, 0, 0) is presumably due to the reduction of the magnetic form factor. Interestingly, our measurements on the (2, 0, 0) reflection at 7.5 T clearly reveal an intensity drop below ~0.3 K (figure 7(b)). This suppression is independent of the emergent AFM order, as the latter sets in at 0.6 K. Although we did not measure the temperature dependence of this reflection at lower fields due to the much weaker signal (0.1–0.2 μ_B/Co [31]), we believe that the suppressed M_z might persist in the IC-AFM region, and be responsible for the discrepancy shown in figure 6(a).

We investigated the transverse spin correlation as a function of magnetic field (figures 6(b) and (c) measured on TriCS and figure 7(a) measured on RITA-II). Unlike the three-dimensional long-range LSDW order in $BaCo_2V_2O_8$ [20], the (2, 3, $\pm\delta l$) peak is not resolution limited along both the *h*- and *k*-directions in $SrCo_2V_2O_8$, which suggests short-range spin correlation in the *ab* plane. Interestingly, the transverse long-range spin correlation is recovered in the emergent AFM state (figure 7(a)). The suppressed longitudinal uniform magnetization M_z and transverse short-range spin correlation indicate that the IC-AFM order in $SrCo_2V_2O_8$ is distinct from the perfect LSDW order observed in $BaCo_2V_2O_8$.

In a TLL with Ising-like anisotropy, the critical magnetic field (H_c) at which the crossover between the longitudinal and transverse spin fluctuations occurs scales linearly with the intrachain exchange strength (J in equation (1)) [22]. The LSDW order in an Ising-like quasi 1D quantum magnet results from the condensation of the longitudinal mode while the interactions between the chains become energetically relevant. An important conclusion revealed by the mean-field theory is that the collapse of the LSDW order does not coincide with H_c, but shifts to a higher value [22]. Therefore, the LSDW order is expected to be more robust in a system with a larger J. Based on the high field magnetization and inelastic neutron scattering investigations, J is larger in $SrCo_2V_2O_8$ than that in $BaCo_2V_2O_8$ [14, 31–34]. However, the IC-AFM order in $SrCo_2V_2O_8$ turns out to be more fragile (figure 5(b)). We note that the experimental critical field for the LSDW to transverse AFM order transition in $BaCo_2V_2O_8$ [24] already deviates from the mean-field prediction in [22]. The even more significant deviation in $SrCo_2V_2O_8$ revealed in our study further stresses the inadequacy of the interchain mean-field theory in addressing the complex magnetism in these systems.

6. Summary

In conclusion, we have employed single-crystal neutron diffraction to map out the magnetic phase diagram of $SrCo_2V_2O_8$ up to 14.9 T and down to 50 mK. As shown in figure 8, our results are in excellent agreement with the previous magnetization and heat capacity investigation on the same crystal [11]. The deviation from the thermal expansion and magnetostriction study, in which the single-crystal was grown by a different method [35], could come from the variation in sample quality. This system is composed of weakly coupled $S = 1/2$ *XXZ* spin chains with Ising-like anisotropy. Like its related counterpart $BaCo_2V_2O_8$, $SrCo_2V_2O_8$ shows multiple magnetic-field-driven

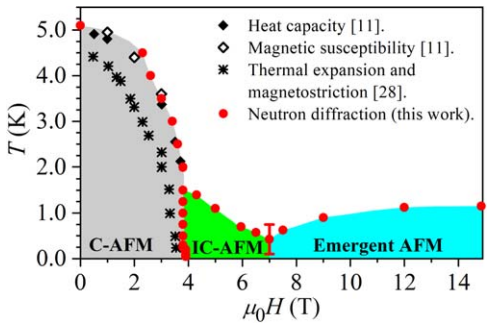

Figure 8. Magnetic field versus temperature phase diagram of $SrCo_2V_2O_8$.

phase transitions that reflect the quantum critical nature of the spins in a TLL state. In addition to the similarity, we have identified several unique signatures for the spin states in $SrCo_2V_2O_8$, including the fragility of IC-AFM order, loss of three-dimensional long-range spin correlation in the IC-AFM region and suppression of uniform magnetization along the *c* axis at low temperatures.

Our observations highlight the complex magnetic properties in these systems and evidence the inadequacy of the interchain mean-field theory. Further investigations, e.g. magnetic refinement, density functional theory calculations and inelastic neutron spectroscopy measurements, are in high demand to shed more lights on the magnetic structures in the C-AFM, IC-AFM, and emergent AFM states, as well as the interchain couplings in $SrCo_2V_2O_8$.

Acknowledgments

We acknowledge the UK EPSRC for funding under grant number EP/J016977/1. This work is based on experiments performed at the Swiss spallation neutron source SINQ, Paul Scherrer Institute, Villigen, Switzerland. One of the authors, Z He thanks the National Natural Science Foundation of China (No. 21573235) and the Chinese Academy of Sciences under Grant No. KJZD-EW-M05 for financial support.

References

[1] Faddeev L and Takhtajan L 1981 *Phys. Lett.* A **85** 375
[2] Lake B, Tsvelik A M, Notbohm S, Alan Tennant D, Perring T G, Reehuis M, Sekar C, Krabbes G and Büchner B 2009 *Nat. Phys.* **6** 50
[3] Kenzelmann M, Chen Y, Broholm C, Reich D H and Qiu Y 2004 *Phys. Rev. Lett.* **93** 017204
[4] Coldea R, Tennant D A, Wheeler E M, Wawrzynska E, Prabhakaran D, Telling M, Habicht K, Smeibidl P and Kiefer K 2010 *Science* **327** 177
[5] Wang Z *et al* 2016 *Phys. Rev.* B **94** 125130
[6] Faure Q *et al* 2018 *Nat. Phys.* **14** 716
[7] Wang Z *et al* 2018 *Nature* **554** 219
[8] Ruegg C, Cavadini N, Furrer A, Gudel H U, Kramer K, Mutka H, Wildes A, Habicht K and Vorderwisch P 2003 *Nature* **423** 62
[9] Giamarchi T, Ruegg C and Tchernyshyov O 2008 *Nat. Phys.* **4** 198
[10] Zapf V, Jaime M and Batista C D 2014 *Rev. Mod. Phys.* **86** 563
[11] He Z, Taniyama T and Itoh M 2006 *Phys. Rev.* B **73** 212406
[12] Bera A K, Lake B, Essler F H L, Vanderstraeten L, Hubig C, Schollwöck U, Islam A T M N, Schneidewind A and Quintero-Castro D L 2017 *Phys. Rev.* B **96** 054423
[13] He Z, Taniyama T and Itoh M 2006 *J. Cryst. Growth* **293** 458
[14] Bera A K, Lake B, Stein W-D and Zander S 2014 *Phys. Rev.* B **89** 094402
[15] Abragam A and Pryce M H L 1951 *Proc. R. Soc.* A **206** 173
[16] Lines M E 1963 *Phys. Rev.* **131** 546
[17] Bethe H 1931 *Z. Phys.* **71** 205
[18] Haldane F D M 1980 *Phys. Rev. Lett.* **45** 1358
[19] Bogoliubov N, Izergin A and Korepin V 1986 *Nucl. Phys.* B **275** 687
[20] Kimura S *et al* 2008 *Phys. Rev. Lett.* **101** 207201
[21] Canévet E, Grenier B, Klanjšek M, Berthier C, Horvatić M, Simonet V and Lejay P 2013 *Phys. Rev.* B **87** 054408
[22] Okunishi K and Suzuki T 2007 *Phys. Rev.* B **76** 224411
[23] Kimura S, Takeuchi T, Okunishi K, Hagiwara M, He Z, Kindo K, Taniyama T and Itoh M 2008 *Phys. Rev. Lett.* **100** 057202
[24] Grenier B, Simonet V, Canals B, Lejay P, Klanjšek M, Horvatić M and Berthier C 2015 *Phys. Rev.* B **92** 134416
[25] Klanjšek M, Horvatić M, Krämer S, Mukhopadhyay S, Mayaffre H, Berthier C, Canévet E, Grenier B, Lejay P and Orignac E 2015 *Phys. Rev.* B **92** 060408
[26] Lefmann K, Niedermayer C, Abrahamsen A, Bahl C, Christensen N, Jacobsen H, Larsen T, Häfliger P, Filges U and Rønnow H 2006 *Physica* B **385–386** 1083
[27] Wills A 2000 *Physica* B **276–278** 680

[28] Kawasaki Y, Ideta Y, Kishimoto Y, Ohno T, Omura K, Fujita T, Kimura S and Hagiwara M 2014 *Proc. Int. Conf. on Strongly Correlated Electron Systems (SCES2013)*
[29] He Z, Taniyama T, Kyômen T and Itoh M 2005 *Phys. Rev.* B **72** 172403
[30] Kawasaki Y *et al* 2011 *Phys. Rev.* B **83** 064421
[31] Okutani A, Kida T, Usui T, Kimura T, Okunishi K and Hagiwara M 2015 *Phys. Proc.* **75** 779
[32] Kimura S, Yashiro H, Okunishi K, Hagiwara M, He Z, Kindo K, Taniyama T and Itoh M 2007 *Phys. Rev. Lett.* **99** 087602
[33] Grenier B, Petit S, Simonet V, Canévet E, Regnault L-P, Raymond S, Canals B, Berthier C and Lejay P 2015 *Phys. Rev. Lett.* **114** 017201
[34] Matsuda M *et al* 2017 *Phys. Rev.* B **96** 024439
[35] Niesen S K, Breunig O, Salm S, Seher M, Valldor M, Warzanowski P and Lorenz T 2014 *Phys. Rev.* B **90** 104419